Spectroscopy of high-lying resonances in ^{9}Be by the measurement of (p, p), (p, d), and (p, α) reactions with a radioactive ^{8}Li beam

E. Leistenschneider,[1,2] A. Lépine-Szily,[1,*] M. A. G. Alvarez,[1,3] D. R. Mendes, Jr.,[4] R. Lichtenthäler,[1] V. A. P. Aguiar,[1] M. Assunção,[5] R. Pampa Condori,[1] U. U. da Silva,[1] P. N. de Faria,[4] N. Deshmukh,[1,6] J. G. Duarte,[1,7] L. R. Gasques,[1] V. Guimarães,[1] E. L. A. Macchione,[1] M. C. Morais,[8] V. Morcelle,[9] K. C. C. Pires,[1] V. B. Scarduelli,[1] G. Scotton,[1] J. M. B. Shorto,[10] and V. A. B. Zagatto[4,1]

[1]*Instituto de Física, Universidade de São Paulo, 05508-090, São Paulo, SP, Brazil*
[2]*The University of British Columbia, Department of Physics and Astronomy, Vancouver, BC V6T 1Z1, Canada*
[3]*Departamento de FAMN, Universidad de Sevilla, Apdo 1065, E-41080, Sevilla, Spain*
[4]*Instituto de Física, Universidade Federal Fluminense, Niterói, RJ, 24210-340, Brazil*
[5]*Departamento de Física, Universidade Federal de São Paulo, Campus Diadema, São Paulo, Brazil*
[6]*Istituto Nazionale di Fisica Nucleare - Laboratori Nazionale del Sud, Catania, Via Santa Sofia, 62, CT - 95123, Italy*
[7]*Dipartimento di Matematica e Fisica, Universit della Campania Luigi Vanvitelli, viale Lincoln, 81100, Caserta, Italy*
[8]*Universidade Federal Fluminense, Instituto do Noroeste Fluminense de Ensino Superior, 28470-000, Santo Antonio de Padua, RJ, Brazil*
[9]*Universidade Federal Rural do Rio de Janeiro, RJ, Brazil*
[10]*Instituto de Pesquisas Energéticas e Nucleares, IPEN, São Paulo, SP, Brazil*

(Received 16 March 2018; revised manuscript received 28 June 2018; published 5 December 2018)

We measured the ^{8}Li$(p, p)^{8}$Li, ^{8}Li$(p, d)^{7}$Li, and ^{8}Li$(p, \alpha)^{5}$He reactions at low energies using the thick target inverse kinematics method, with a polyethylene $[CH_2]_n$ target and a radioactive ^{8}Li beam available at the Radioactive Ion Beams in Brazil facility of São Paulo. By measuring simultaneously several reaction channels (p, p), (p, d), and (p, α), the still uncertain high-lying resonances of ^{9}Be, close to the proton threshold, can be studied and their parameters, such as energy, width, and spin parity can be more reliably determined. The experimental excitation functions of the reactions ^{8}Li$(p, p)^{8}$Li, ^{8}Li$(p, d)^{7}$Li, and ^{8}Li$(p, \alpha)^{5}$He were analyzed using the R-matrix theory, which allows us to infer the properties of the resonances. Multichannel R-matrix analysis provides evidence for a significant clustering in the (p, d) channel. The experimental data and the multichannel R-matrix analysis will be presented.

DOI: 10.1103/PhysRevC.98.064601

I. INTRODUCTION

The study of weakly bound nuclei, radioactive or stable, is of permanent interest in nuclear structure and in nuclear reactions and the study of nuclei far from the stability valley, also called exotic, is at the forefront of current research in nuclear physics [1]. Facilities that produce beams of radioactive nuclei are being developed worldwide, and provide unique opportunities to probe new aspects of nuclear physics [2–4] and of nuclear astrophysics [5], as the existence of halo nuclei or the emergence of new magic numbers, among others.

The concept of exoticism can be extended by considering either core excitations, or a larger number of cluster constituents. Recently, core excitation has been observed by inelastic scattering in ^{18}Ne + p [6]. Modern scattering calculations also involve core excitations, as an important contribution to the reaction mechanism [7,8]. On the other hand, most exotic nuclei present a two- or three-body structure. Some nuclei, such as ^{10}C, can even be considered as Borromean four-body systems (none of the two- or three-body substructures of the $\alpha + \alpha + p + p$ system is bound), but there is currently no experimental evidence for four-body clustering.

In the present work, we intend to investigate exotic states in ^{9}Be, near the proton threshold, possibly characterized by a multicluster structure. At low proton energies, we probe the ^{9}Be spectrum around $E_x \approx 18$–20 MeV. This energy region was previously studied by our group [9] (see also Erratum [10]), but was limited to the ^{8}Li$(p, \alpha)^{5}$He cross section. To this aim, we use three reactions involving a radioactive ^{8}Li beam on a proton target. By observing simultaneously the protons, the deuterons and the α particles, we determine the excitation functions of the ^{8}Li$(p, p)^{8}$Li elastic scattering, and the ^{8}Li$(p, d)^{7}$Li and ^{8}Li$(p, \alpha)^{5}$He transfer reactions.

The excitation functions of the ^{8}Li$(p, p)^{8}$Li, ^{8}Li$(p, d)^{7}$Li, and ^{8}Li$(p, \alpha)^{5}$He reactions were analyzed by the R-matrix theory [11,12]. It is a very convenient method to analyze low-energy data. It introduces poles to describe bound states and resonances in the excitation functions. The R-matrix parameters, energies, and reduced widths, are associated with properties of ^{9}Be states. The simultaneous analysis of different reaction channels with common parameters provides constraints on these parameters.

*alinka@if.usp.br

The paper is organized as follows. In Sec. II, we present the experimental setup and method. Section III is devoted to experimental data analysis and results. In Sec. IV is presented the R-matrix analysis of the data, and a discussion of ^{9}Be spectroscopy near the proton threshold. Concluding remarks and outlook are presented in Sec. V. In an Appendix we give all details about possible contamination in our experiment.

II. EXPERIMENTAL METHOD

A. RIBRAS facility and production of ^{8}Li beams

The reactions of the $^{8}\mathrm{Li} + p$ system were studied with the Radioactive Ion Beams in Brazil (RIBRAS) facility, installed at the 8-UD Pelletron Tandem of the University of São Paulo. The details can be found in Refs. [4,9,13,14] and a schematic overview of the RIBRAS system can be seen at Fig. 1. The facility consists of two superconducting solenoids with 6.5 T maximum central field and a 30 cm clear warm bore, a production target mounted in chamber (1) before the first solenoid, a central scattering chamber (2) between the two solenoids, and a large scattering chamber (3) after the second solenoid. Both chambers (2) and (3) have target towers that can hold up to four target foils and frames for ΔE-E Si telescopes to detect particles scattered or produced on the targets.

The $^{7}\mathrm{Li}^{3+}$ primary beam was accelerated by the Pelletron Accelerator at energy of 24.4 MeV, and its current on the production target was typically 300 nA. The primary beam (^{7}Li) was stopped after the production target in a Faraday cup, constituted by an isolated tungsten rod, which stops all particles in the angular region from $0^{\circ}-2^{\circ}$, and where the primary beam intensities are integrated.

The $^{8}\mathrm{Li}^{3+}$ beam with $E = 22.5$ MeV was produced by the ^{9}Be(^{7}Li, ^{8}Li)^{8}Be one-neutron transfer reaction ($Q = 0.367$ MeV) with a ^{9}Be foil of 16 μm thickness as production target. The tungsten stopper and a collimator at the entrance of the first solenoid define the angular acceptance of the system, which in the present experiment was, respectively, 4° (between 2° and 6°) in the entrance of the first solenoid, and 2° (between 1.5° and 3.5°) at the exit of the second solenoid. The angular straggling in targets and degraders will increase the angular divergence of the secondary beam and this will be detailed for each target and degrader in the following.

The secondary beams are selected and focused by the solenoids according to their magnetic rigidity. The ^{8}Li beam transport to each of the chambers (2) and (3) was optimized by varying the current of the corresponding solenoid and maximizing the ^{8}Li detected in a ΔE-E Si telescope after its elastic scattering on a ^{197}Au target mounted in the respective chamber (2) or (3).

The radioactive ^{8}Li beam can be purified after the second solenoid by passing through a degrader mounted in chamber (2), which changes the magnetic rigidity of the beam of interest and contaminant beams by different amounts. The method was tested previously with ^{8}Li beam scattering in a ^{197}Au target of 5.3 mg/cm^2 thickness and detected by a ΔE-E Si telescope with thicknesses of 50 μm and 1000 μm, respectively, in chamber (3), without and with a 4.6 mg/cm^2 $[CH_2]_n$ degrader mounted in chamber (2). The identification spectra obtained in this test were published in Refs. [4,14]. The degrader eliminated nearly all contaminant beams, and the result was a 99% pure ^{8}Li secondary beam in chamber (3). In our experiment, to avoid possible recoil protons from $[CH_2]_n$ degrader in our proton spectra, we changed the material to aluminum. The thickness of the degrader was calculated by the code SIM-RIBRAS [15], which optimizes the purity of the beam and calculates the currents in the solenoids. The ^{8}Li beam with energy of 16.0 MeV stops in the 50 μm ΔE detector after passing through the ^{197}Au target of 5.3 mg/cm^2. We obtained purity of 98.4% of ^{8}Li with 0.69% of ^{4}He, 0.9% of ^{3}H and 0.01% of ^{1}H as contaminants in our experiment with the Al degrader.

B. Scattering setup for cross-section measurements

The measurements of the $^{8}\mathrm{Li} + p$ cross sections were performed in the scattering chamber (3) after the second solenoid, with a pure ^{8}Li secondary beam of 16.0 MeV hitting a thick $[CH_2]_n$ polyethylene target of 6.7 mg/cm^2. The reactions were measured in inverse kinematics, which yields low energies in the center of mass reference frame.

Targets of ^{197}Au and natural carbon were also mounted, respectively, with thicknesses of 5.3 and 15.0 mg/cm^2. Measurements of Rutherford elastic scattering ^{197}Au(^{8}Li, ^{8}Li) with the gold target were performed several times in order to normalize the ^{8}Li beam intensity, and the production rate was quite constant (about 2×10^{4} pps). Measurements with the natural carbon target were also performed in order to subtract possible reactions with the carbon present in the polyethylene target.

The particles produced by the secondary beam on the reaction targets were detected using a ΔE-E Si telescope with thicknesses of 50 μm and 1000 μm, respectively, covering

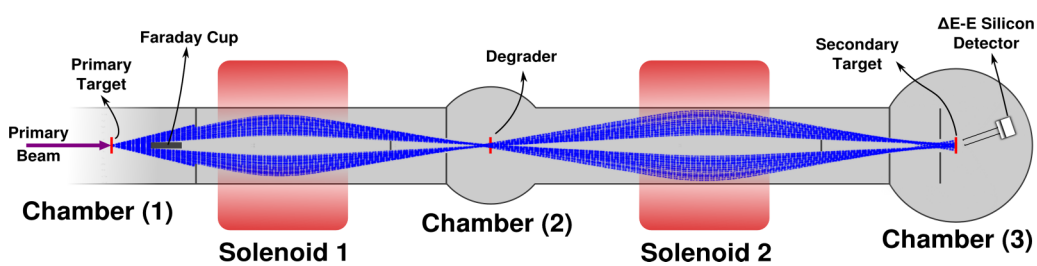

FIG. 1. Schematic overview of the RIBRAS facility depicting its main components. Blue lines are simulated trajectories of secondary beam transport through the setup.

a geometrical solid angle of 12.0 msr. A large vertical Al blocker, with a 3.5 cm diameter hole, aligned with the target of 2 cm diameter, was placed 2 cm before the target holder in order to clean the beam from contaminant ions arriving into the target with different trajectories (see Fig. 1). A set of collimators in front of the telescope prevented that contaminant beams with different trajectories reach the detectors. The basis of the chamber consists of double, independently rotating plates. For the ^{8}Li + p measurements the Si telescope was located at $\theta_{lab} = 18^{\circ}$, which was a safe position with no contamination in the measured spectra. The detectors were calibrated using a standard α-particle source.

The angular divergence of the beam in the center of chamber (2), before the degrader, is the divergence related to the solenoid geometry (1.3°–5.5°), thus 3.2°. The ^{8}Li beam of 22.5 MeV and this divergence impinges on the Al degrader of 7.5 mg/cm^2. The total divergence after the degrader was calculated as the quadratic sum of the original divergence 3.2° with the angular straggling of the ^{8}Li beam passing through the Al degrader (3.26°). This calculation yielded FWHM = 4.5° around the average angle of ±2.9°. This is the angular divergence of the beam incident on the target localized in the center of chamber (3). For the thick $[CH_2]_n$ polyethylene target, the angular spread of the beam (which stops in the target) has not much effect on the data since we are detecting the backward center of mass angles, where the direct contribution to the reaction should be negligible. The localization of the reaction spot can be larger by a small amount and consequently the energy resolution of the light particles.

For the Au target the effect is much more important. The angular straggling in the Au target is FWHM = 5.7°. Performing the quadratic sum of the two factors, we obtain FWHM = 7.3° around ±2.9°, or a beam with total angular opening of ±6.55° after having passed through the Al degrader and the Au secondary target. The detection angle is $\theta_{lab} = 18^{\circ} \pm 2^{\circ}$. If the undiverted beam can emerge from the target at ±6.55° than the smallest and largest scattering angles can be, respectively, 9.5° and 26.5°, and they can enter into the telescope, when the geometrical average angle of the telescope = 18 ± 2°. The determination of the effective average scattering angle is of foremost importance. The Rutherford elastic scattering of ^{8}Li on Au is assumed to determine the number of incident beam particles on the target and such Rutherford cross section has a rapid variation with the scattering angle. This concept is mainly important for radioactive ion beams produced, in flight, by transfer reactions [4], due to the large angular divergence of the beam scattered on a detector with large angular opening, positioned at forward angles. Further details can be found in Ref. [4] and in other publications realized with a similar technique at RIBRAS [9,13,14,16–26].

The ΔE-E Si telescope in use was moved during the experiment to measure the ^{8}Li + ^{197}Au angular distribution. It is presented on Fig. 2(a). When the geometrical scattering angle was considered the cross section increased above the Rutherford cross section at forward angles. A Monte Carlo simulation was developed to solve this problem, which takes into account the collimator size, the secondary beam spot

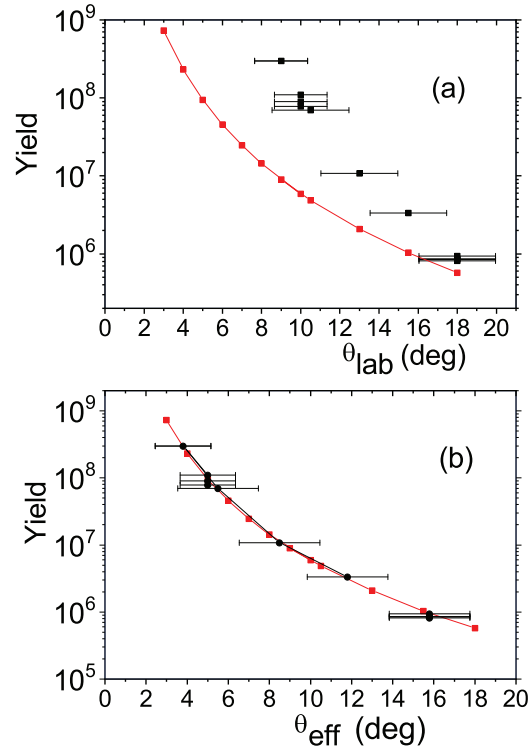

FIG. 2. (a) The yield of the experimental ^{8}Li + ^{197}Au angular distribution is presented by black squares. The red line is the Rutherford cross section. (b) Using the effective average scattering angle instead of the geometrical one, the angular distribution agrees with the Rutherford cross section.

size ($\phi = 7$ mm), the secondary beam divergence, the angular straggling in the degrader and secondary target, and the angular distribution of the emitted particles. It yields the effective average detection angle, the total angular uncertainty ($\sigma_{ang} = 2.2^{\circ}$) and the effective solid angle. The effective average detection angle is calculated as the weighted average angle, where the weight is given by the number of particles arriving/unit angle, or weighted by the Rutherford differential cross section, in our case. Its calculated value was $\theta_{eff} = 15.7^{\circ}$ for $\theta_{lab} = 18^{\circ}$. The experimental angular distribution on gold confirmed the angular shift in calculated angle values. We show on Fig. 2(b) that using the effective angles instead of the geometrical ones the measured angular distribution followed the Rutherford behavior, proving the correctness of the calculations. The angular correction was very important for the gold target and for the calculation of the ^{8}Li beam intensity. It is important to mention that the angular dependence of the ^{8}Li(p, p)^{8}Li, ^{8}Li(p, d)^{7}Li, and ^{8}Li(p, α)^{5}He reactions is much weaker than the Rutherford cross section and for these reactions we assume $\theta_{eff} = \theta_{lab} = 18^{\circ}$.

C. Thick target inverse kinematics method and results

The measurement of the ^{8}Li(p, p)^{8}Li, ^{8}Li(p, d)^{7}Li, and ^{8}Li(p, α)^{5}He excitation functions was performed using the so-called thick target inverse kinematics (TTIK) method, with a ^{8}Li secondary beam impinging on a 6.7 mg/cm^2 thick

$[CH_2]_n$ polyethylene foil. The reaction between the ^{8}Li and the target protons can form the compound system ^{9}Be. The ^{8}Li loses energy in the target until it stops, and the reaction is performed continuously at all energies from the maximum energy down to zero. Whenever a resonance in ^{9}Be is populated, a larger number of p, d, and α particles can be produced and detected in the Si telescopes, producing a peak in the respective spectra. The energy spectra of the emitted light particles, protons, deuterons, and α particles thus corresponds to the excitation functions of the reactions (p, p), (p, d), and (p, α).

The great advantage of the method is the good energy resolution, which does not depend on the energy dispersion of the incident ^{8}Li beam, which in the present experiment was $\sigma(^8\text{Li}) = 370$ keV, measured by the elastic scattering peak on the ^{197}Au target in chamber (3). The ^{8}Li beam particles having different energies in the beam envelope, will perform the same reaction at slightly different points in the target, but the light particles emitted have the same energy. The energy dispersion in the detected energy will be due to the slightly different energy loss of the light particles as they travel different distances in the target. As the energy loss of the light particles is quite small, the resolution will be very good. We calculated this energy resolution, converting the energy dispersion of the ^{8}Li beam into a distance Δx through its stopping power dE/dx and reconverting Δx into the energy dispersion of the protons, deuterons, and α particles, using their respective stopping powers. The energy resolution of the light particles was $\sigma(p) = 16$ keV, $\sigma(d) = 23$ keV, and $\sigma(\alpha) = 56$ keV. The energy variation of the resolution is related to the energy variation of the stopping power: as the Bragg peak of the light ions is situated at very low energies, for higher incident energy the light particles will have higher energy and lower stopping power, resulting in better resolution.

The maximum energies of the protons, deuterons, and α particles, from the reactions $^8\text{Li}(p, p)^8\text{Li}$, $^8\text{Li}(p, d)^7\text{Li}$, and $^8\text{Li}(p, \alpha)^5\text{He}$, detected at $\theta_{\text{lab}} = 18^\circ$, are respectively $E_p(\text{detector}) = 5.15$ MeV, $E_d(\text{detector}) = 7.06$ MeV, $E_t(\text{detector}) = 4.5$ MeV, and $E_\alpha(\text{detector}) = 26.0$ MeV taking into account the energy losses in the target.

Protons, deuterons, and tritons stop in the 50 μm ΔE detector with energies, respectively, less than 2, 4, and 6 MeV. The electronic noise pollutes the proton and deuteron spectra up to 3.5 and 5 MeV. Thus we do not observe the tritons from the $^8\text{Li}(p, t)^6\text{Li}$ reaction in our spectra. The light ejectiles, protons, deuterons, and α particles were detected at forward laboratory angle 18°, which corresponds for the elastic scattering to the backward center of mass angle 144°.

On Fig. 3 (top) we present the bidimensional identification spectrum of the Si telescope at $\theta_{\text{lab}} = 18^\circ$, using the thick $[CH_2]_n$ target. We clearly see well-separated proton, deuteron, triton, and α strips. In this measurement we had 4.5×10^8 incident ^{8}Li beam particles. We also measured in the same conditions, spectra using the gold and the carbon targets, in order to see the possible contaminant beams, and the contaminant reactions on the carbon content of the polyethylene foil. On the gold target (Fig. 3, middle), with 0.85×10^8 incident ^{8}Li beam particles, there are no protons and deuterons, only α particles and tritons (two spots), with well-defined energies. They represent the 1.6% contamination in the purified ^{8}Li beam. On the carbon target, we performed measurements with 8.2×10^8 incident ^{8}Li beam particles. We can see qualitatively, that there are very few α particles, tritons, and deuterons, and somewhat more protons. In the next section we give our conclusions about possible contaminations.

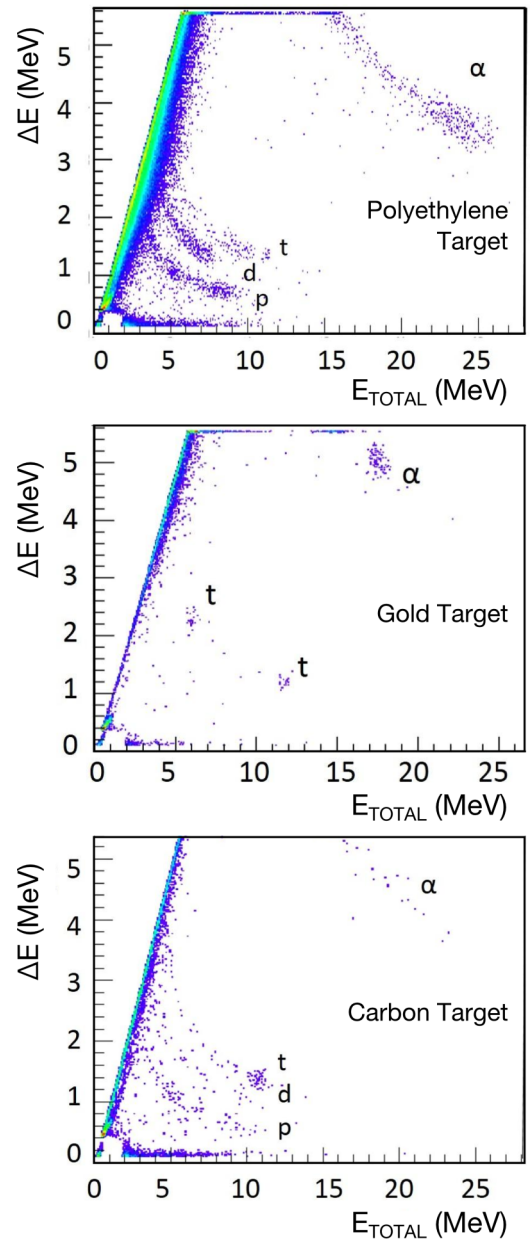

FIG. 3. Bidimensional identification spectra obtained using a Si telescope at $\theta_{\text{lab}} = 18^\circ$ in the scattering chamber (3), with the secondary beam of $E_{\text{lab}} = 16.0$ MeV. We clearly see well-separated proton, deuteron, triton, and α strips. The beam was focused, respectively, on: the $[CH_2]_n$ target of 6.7 mg/cm^2 (top), with 4.5×10^8 incident ^{8}Li beam particles; a ^{197}Au target of 5.3 mg/cm^2 (middle) with 0.85×10^8 incident ^{8}Li beam particles; a carbon target of 15 mg/cm^2(bottom) with 8.2×10^8 incident ^{8}Li beam particles.

D. Possible contamination

We list all possible reactions between the possible beams arriving on the target (^{8}Li, d, t, α) and the target constituents (p, ^{12}C). We calculated their kinematics, and determined the energy range of light ejectiles as protons, deuterons, and α particles arriving in our detector. We give the conclusions in this section and all details are presented in the Appendix, at the end of the paper. Table II in the Appendix has all possible reactions and their energy range in the detectors.

The proton spectrum has no contamination in the energy range of interest between E_p(detector) = 3.5−5.15 MeV, however the protons we observed with energies between 5.2 and 10.5 MeV can come from ^{1}H(α, p)^{4}He, ^{1}H(t, p)^{3}H, and ^{12}C(α, p)^{15}N reactions.

The maximum detected deuteron energy is about 7.5 MeV, which is close to the kinematic limit of the (p, d) reaction of interest. The possible contaminant reactions should yield higher energy deuterons, so we can conclude that they are not observed. This conclusion is also supported by the very low yield of deuterons (and α's) on the carbon target, which had similar number of incident particles.

The same argument supports that the α spectrum is also free from contamination. α particles produced with energy below 18 MeV are out of the region measured with purified ^{8}Li beam, presenting no harm to our data.

III. DATA ANALYSIS

The energy of the light particles detected in the Si telescopes depends on the detection angle, on the target thickness, and on the incident energy of the ^{8}Li beam. In order to transform these energies into center-of-mass energy of the ^{8}Li + p system, we performed simulations, using the following procedure. The thick target was divided into thin slices of 0.1 mg/cm^2. The energy of the ^{8}Li beam at the end of each slice was calculated by subtracting the energy loss from the incident energy. Then the energy of the emitted light particle (p, d, t, α) was obtained from the kinematics of the respective two-body reaction, followed by the energy loss calculation of the light particles in the rest of the target. This calculation yielded the correspondence between the detected light particle energy and ^{8}Li energy, as a function of the angle and incident energy. The center of mass energy of ^{8}Li + p system can be easily calculated from ^{8}Li laboratory energy. However, the transformation would be wrong if the recoiling heavier particle was excited. Thus for the ^{8}Li$(p, d)^7$Li channel, where the recoiling ^{7}Li could be excited, we present the energy spectra not as a function of $E_{\rm c.m.}$, but of the light particle's laboratory energy immediately after the reaction. This energy can also be obtained from the same simulation.

The differential cross section in the center of mass frame is calculated using

$$\frac{d\sigma}{d\Omega}(E,\theta)_{\rm c.m.} = \frac{NJ}{\Delta\Omega N_{\rm inc} N_{\rm target}}, \qquad (1)$$

where N is the total number of light particles detected with energy corresponding to the interval E and $E + \Delta E(^8\text{Li})$, $\Delta\Omega$ is the solid angle of the detector considered, $N_{\rm inc}$ is the number of ^{8}Li ions incident on the secondary target, J is the Jacobian that converts the geometrical solid angle from the laboratory frame to the center of mass frame. The number of target atoms per unit area, $N_{\rm target}$, is not constant, since the energy loss of the beam, $\Delta E(^8\text{Li})$ per unit distance Δx, depends on the energy. $N_{\rm target}$ is calculated using

$$N_{\rm target} = \frac{\Delta E(^8\text{Li})}{\frac{dE}{dx}}. \qquad (2)$$

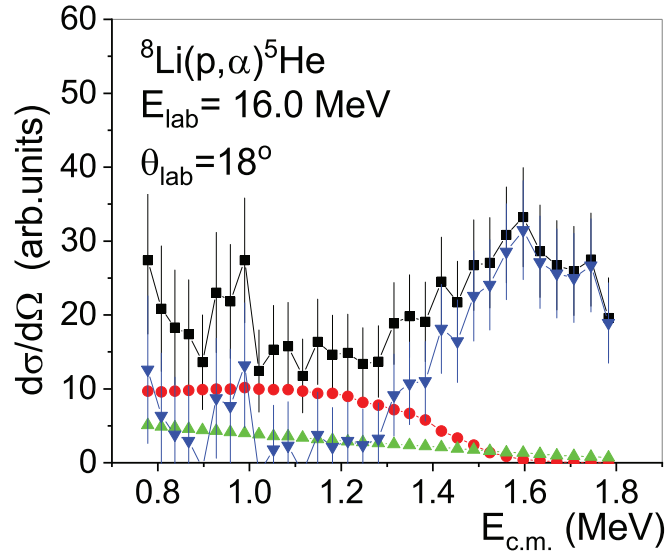

FIG. 4. The experimental cross section of the reaction ^{8}Li$(p, \alpha)^5$He before (black dots) and after (blue triangles) the subtraction of the α particles from the decay of ^{5}He (red dots), and of the phase-space three-body breakup (green triangles).

Details on the analysis method of the ^{8}Li$(p, \alpha)^5$He reaction can be found in Ref. [9]. This reaction needs some special attention, since the recoiling ^{5}He is unbound and breaks up into an α particle and a neutron. Observing the variation with angle of the resonance energy (centroid), at $E_{\rm c.m.}$ = 1.7 MeV, and comparing with two-body kinematics, we have shown that the ^{1}H(^{8}Li, $\alpha)^5$He reaction was a two-body reaction [9]. Most of the breakup of ^{5}He occurs, when the ^{4}He ejectile and the recoiling ^{5}He are moving away. This finding is in agreement with the half-life of the ^{5}He ground state ($T_{1/2} = 1 \times 10^{-21}$ s). Similarly, in the ^{1}H(^{8}Li, ^{8}Be)n reaction the ^{8}Be is unbound breaking into two α particles, and their energy and kinematic angular variation does not agree with the observation. The contribution of the breakup α particles, as well as the continuous energy distribution of α particles resulting from the phase-space three-body breakup, were calculated and subtracted from the energy spectra.

In Fig. 4 we present our cross section for the reaction ^{8}Li$(p, \alpha)^5$He without the subtraction of backgrounds (black dots), the background due to α particles from the decay of ^{5}He (red dots), the background due to the phase-space three-body breakup (green triangles) and the final cross section after the subtraction of backgrounds (blue triangles). This subtraction affects mainly the form and the width of the peak, and thus

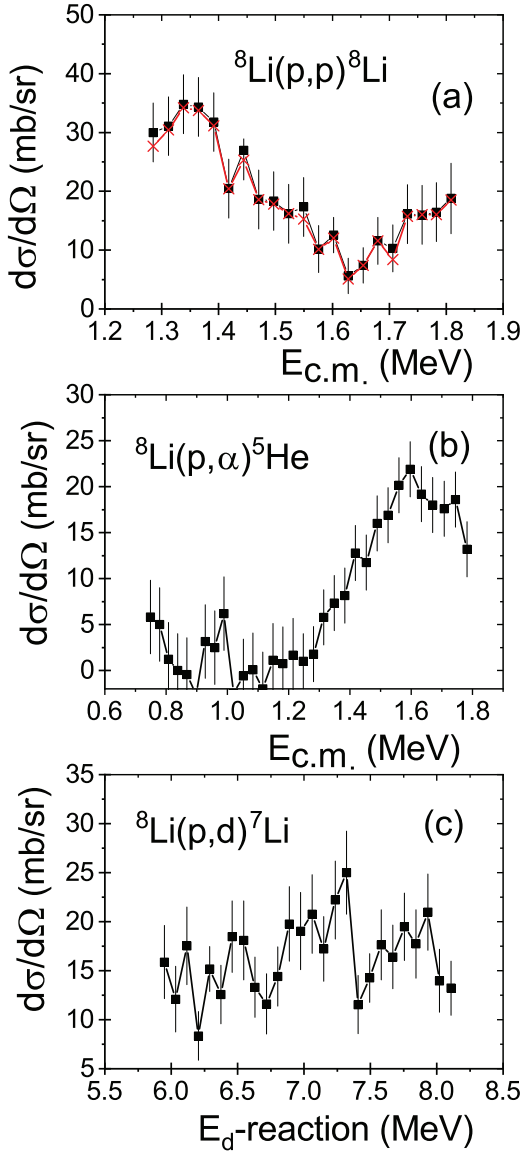

FIG. 5. The experimental cross sections of the reactions (a) ^{8}Li$(p, p)^8$Li, (b) ^{8}Li$(p, \alpha)^5$He, and (c) ^{8}Li$(p, d)^7$Li measured at $\theta_{lab} = 18^\circ$ with the secondary beam of $E_{lab} = 16.0$ MeV. The black dots and red crosses in (a) were obtained, respectively, without and with the subtraction of the background of protons detected with Carbon target.

is very important for a correct determination of the resonance parameters.

The cross sections for the reactions ^{8}Li$(p, p)^8$Li, ^{8}Li$(p, d)^7$Li, and ^{8}Li$(p, \alpha)^5$He were calculated following Eqs. (1) and (2). For the proton spectrum we subtracted the proton background measured with carbon target. For the deuteron spectrum no background was subtracted and for the α spectrum the subtraction explained above and shown on Fig. 4 was performed.

A. Results

In Fig. 5 we present our cross sections for the reactions ^{8}Li$(p, p)^8$Li, ^{8}Li$(p, d)^7$Li, and ^{8}Li$(p, \alpha)^5$He measured at

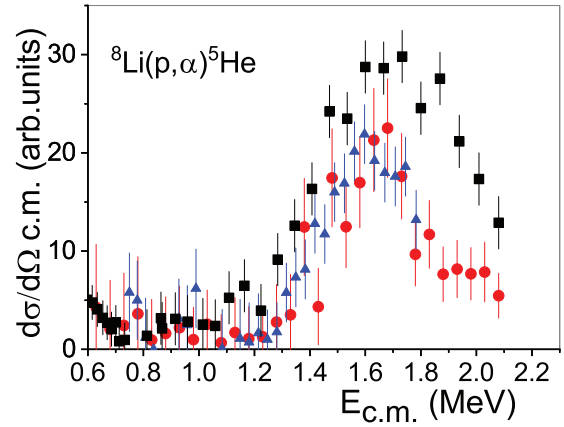

FIG. 6. The superposition of the experimental ^{8}Li$(p, \alpha)^5$He cross sections measured in three experiments is presented. The red dots represent the cross section of ^{8}Li$(p, \alpha)^5$He measured at $E_{lab} = 18.7$ MeV and $\theta_{lab} = 10^\circ$ [27]. The black squares correspond to the ^{8}Li$(p, \alpha)^5$He measurement of Mendes *et al.* [9] (see also Erratum [10]). The blue triangles represent the cross sections shown on Fig. 5(b).

$E_{lab}(^8\text{Li}) = 16.0$ MeV and at $\theta_{lab} = 18^\circ$. The black dots and red crosses of the ^{8}Li$(p, p)^8$Li cross section of Fig. 5(a) were obtained, respectively, without and with the subtraction of the background due to protons detected with carbon target. The ^{8}Li$(p, \alpha)^5$He cross section of Fig. 5(b) was obtained by the subtraction of the decay and phase-space backgrounds shown on Fig. 4. The ^{8}Li$(p, d)^7$Li cross section had no background due to contamination (see Fig. 3) and phase-space decay.

In the ^{8}Li$(p, p)^8$Li data [Fig. 5(a)] we see a strong minimum at $E_{c.m.} = 1.63$ MeV, which is close in energy to the strong peak we observe in the ^{8}Li$(p, \alpha)^5$He data [Fig. 5(b)]. On the other hand, on the ^{8}Li$(p, d)^7$Li channel [Fig. 5(c)], data suggest the presence of two peaks around E_d(reaction) = 7.1 and 7.8 MeV.

The absolute normalization of the cross section at $\theta_{lab} = 18^\circ$ with the secondary beam of $E_{lab} = 16.0$ MeV was obtained from the measurements of the Rutherford elastic scattering of the ^{8}Li beam on a gold target in chamber (3). The elastic angular distribution allowed us to determine correctly the effective scattering angle, independently from calculations.

B. Previous measurements and results

In Figs. 6 and 7 we present the results of our previous measurements. We have measured the same reactions of the $^8\text{Li} + p$ system, using $E_{lab} = 18.7$ MeV and $\theta_{lab} = 10^\circ$ [27] with a purified ^{8}Li beam. In Fig. 6 is shown, using red dots, the ^{8}Li$(p, \alpha)^5$He cross section in arbitrary units, where again, we see the large peak around $E_{c.m.} = 1.65$ MeV. In this measurement we could not obtain the $^8\text{Li} + ^{197}\text{Au}$ angular distribution and determine the effective scattering angle, thus the absolute normalization is uncertain. In Fig. 6 is represented with black squares the cross section of the ^{8}Li$(p, \alpha)^5$He reaction at $\theta_{lab} = 13.5^\circ$, measured with an incident ^{8}Li beam of $E_{lab} = 19.0$ MeV [9] (see also Erratum [10]). In Fig. 6 we show

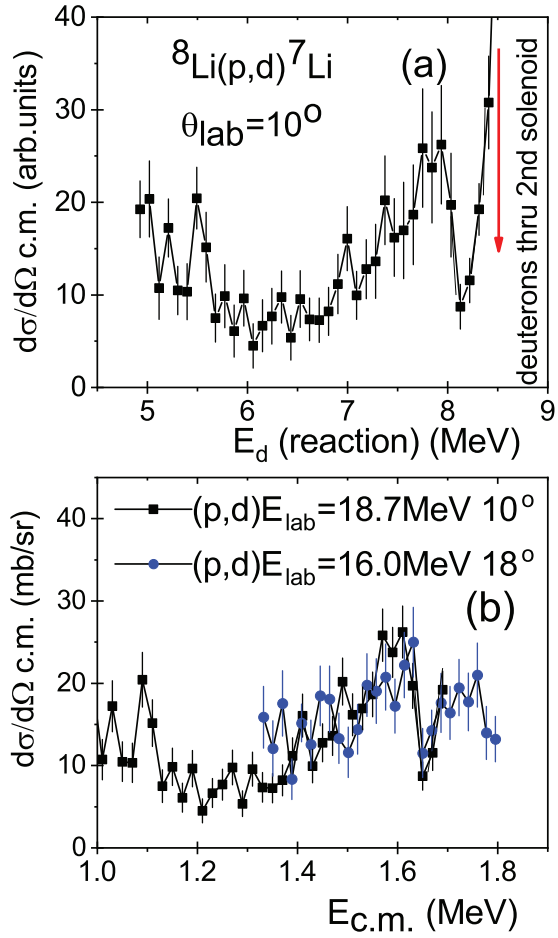

FIG. 7. (a) The cross section of ^{8}Li$(p, d)^7$Li measured at $E_{\rm lab} = 18.7$ MeV and $\theta_{\rm lab} = 10^\circ$ [27]. (b) The comparison, as a function of $E_{\rm c.m.}$, of two measurements of the reaction ^{8}Li$(p, d)^7$Li at different incident energies and angles.

the superposition of all three measurements of ^{8}Li$(p, \alpha)^5$He, the one on Fig. 5(b), with $E_{\rm c.m.} \leqslant 1.786$ MeV and those on Fig. 6 with $E_{\rm c.m.} \leqslant 2.08$ MeV and 2.11 MeV, respectively. All three correspond clearly to the same resonance, but there are differences in width and absolute value.

The difference with the red dot data points of Fig. 6 can be accounted on its problems in the absolute value. The disagreement between the width and the absolute value of the black squares, data of Mendes *et al.* ($E_{\rm lab} = 19.0$ MeV) and our recent data, blue triangles, ($E_{\rm lab} = 16.0$ MeV) will be discussed in more detail in the next section.

In Fig. 7(a) we present the energy spectrum of the detected deuterons measured using $E_{\rm lab} = 18.7$ MeV and $\theta_{\rm lab} = 10^\circ$ [27]. The energy axis is the deuteron energy at the reaction in the target. A strong peak appears at 8.5 MeV. It corresponds to the elastic scattering of a contaminant deuteron beam, focused by the second solenoid, on the proton target. Next to it, at 7.7 MeV, appears a smaller peak corresponding to the reaction ^{8}Li$(p, d)^7$Li. At E_d(reaction) $= 5.5$ MeV another peak is visible, which corresponds to $E_{\rm c.m.} = 1.1$ MeV. There is a resonance at this energy quoted in the literature [28], which was not observed in the ^{8}Li$(p, \alpha)^5$He reaction.

In Fig. 7(b) we superimpose the recent and the previous ^{8}Li$(p, d)^7$Li cross sections, measured at different energies and different angles. When plotted as function of $E_{\rm c.m.}$ (the conversion from deuteron energy to $E_{\rm c.m.}$ was performed assuming the recoiling ^{7}Li in its ground state), the lower-energy peaks coincide in position around $E_{\rm c.m.} = 1.6$ MeV. The higher-energy peak is covered by the contamination in the previous data, but is clearly observed in our recent measurement at $E_{\rm c.m.} = 1.75$ MeV. The remarkable superposition of the peaks as a function of $E_{\rm c.m.}$ reinforce the existence of two peaks in the ^{8}Li$(p, d)^7$Li spectrum.

A measurement of the ^{8}Li$(p, d)^7$Li angular distribution at $E_{\rm c.m.} = 4.0$ MeV has been performed recently by Li Yun-Ju *et al.* [29], and suggests that the ^{7}Li ground and first excited states are equally populated. These data, however, are measured at a different center of mass energy and do not provide information on the resonance structure.

There are two possible interpretations for the existence of two peaks in the ^{8}Li$(p, d)^7$Li channel. One is that the two peaks are due to two channels leading to ^{7}Li$_{\rm gs}$ and ^{7}Li* recoiling nuclei. Performing the kinematic calculation of the energies of the deuterons emitted from the ^{8}Li$(p, d)^7$Li and ^{8}Li$(p, d)^7$Li* reactions, leading to ^{7}Li$_{\rm gs}$ and its first excited state at 0.4776 MeV at $E_{\rm lab} = 16.0$ MeV and $\theta_{\rm lab} = 18^\circ$, respectively, we find E_d(reaction) $= 7.8$ and 6.8 MeV. Thus this energy separation is about 300 keV larger than the distance between the observed peaks.

The second interpretation is of the existence of two resonances in the compound nucleus ^{9}Be, as it was already suggested in our previous work [9], with $E_r = 1.69(3)$ with $\Gamma_{\rm total} = 680(90)$ keV and $E_r = 1.76(4)$ with $\Gamma_{\rm total} = 490(80)$ keV, respectively. If the energy difference between the two resonances is $\Delta E_{\rm c.m.} = 155$ keV, it yields an energy difference between the two peaks in the deuteron spectrum of $\Delta E_{\rm lab}(d) = 155 * (9/2) = 700$ keV. Those peaks would then correspond to $E_{\rm c.m.} = 1.6$ and 1.75 MeV in the ^{8}Li $+ p$ system. However, these resonances should be considerably narrower than the ones found in the previous work, to correspond to the Fig. 7(b).

The first interpretation (the two peaks are due to two channels leading to ^{7}Li$_{\rm gs}$ and ^{7}Li* recoiling nuclei) would be a very important result, with the structure of the ^{9}Be resonance having an excited ^{7}Li* core coupled with a deuteron. The second interpretation also leads to a very relevant conclusion, because it clearly proves the existence of two close-lying resonances at high excitation energies in ^{9}Be.

The published cross section [9] is affected by an unnecessary normalization factor $dE(^8\text{Li})/dE_\alpha$, associated with the conversion from the α energy to the ^{8}Li energy and its removal reduces the cross section (see Erratum [10]). Thus, in Fig. 6 we present the ^{8}Li$(p, \alpha)^5$He cross section without this normalization.

IV. *R*-MATRIX ANALYSIS OF THE DATA

The *R*-matrix theory [11,12] is an ideal tool to analyze low-energy data. It is based on the existence of two regions, separated by the channel radius a. In the internal region, the physics of the problem is described by real and energy-

independent parameters. In the external region, the colliding nuclei interact through the Coulomb force only. The R-matrix parameters, energies and reduced widths, are associated with properties of states of the compound system, in our case, the ^{9}Be. The simultaneous analysis of (p, p), (p, d), and (p, α) data with common parameters provides constraints on these parameters. For example, the energies and proton widths of the resonances are common to the three processes.

Information on clustering or, in other words, on the deformation of a state, can be inferred from the reduced widths γ^2 in the various channels. When γ^2 exhausts a significant fraction (typically $\approx$ 10–20%) of the Wigner limit ($\gamma_W^2 = 3\hbar^2/2\mu a^2$, where μ is the reduced mass), the reduced width brings out a dominant cluster structure in the corresponding channel. This method has been mostly used in elastic and inelastic scattering to investigate proton-rich nuclei [6,30].

In its ground state, ^{9}Be can be accurately described by an $\alpha + \alpha + n$ three-body model [31]. This structure corresponds to a Borromean system, for which none of the two-body subsystems ($\alpha + \alpha$ and $\alpha + n$) is bound. At high excitation energies (the proton threshold energy is $Q_p = 16.89$ MeV), the ^{9}Be spectrum is, however, more complex, and other cluster structures can be expected. The availability of (p, p), (p, d), and (p, α) cross sections obtained simultaneously in the same energy range provides an excellent opportunity to probe the ^{9}Be structure in this energy region.

The present cross sections are then analyzed in terms of a multichannel R-matrix calculation. In this way the transfer to excited state of ^{7}Li and of ^{5}He can also be included among the channels For a given partial wave J^π, the R matrix involving the initial channel i and the final channel f is given by

$$R_{if}(E) = \sum_{\lambda=1}^{N} \frac{\gamma_i^\lambda \gamma_f^\lambda}{E_\lambda - E}, \tag{3}$$

where index λ refers to the N poles, associated with resonances and bound states. The energies are denoted as E_λ, and the reduced partial widths in channel c as γ_c^λ. The present analysis involves five channels: proton ($c = 1$), α ($c = 2$), α' ($c = 3$), d ($c = 4$), and d' ($c = 5$).

The R-matrix parameters $(E_\lambda, \gamma_c^\lambda)$ are real and energy independent. They are specific to the R-matrix theory, and depend on the channel radius. They can be transformed into observed parameters, the resonance energies E_r and the partial widths Γ_c, by well-known techniques [32].

From the R-matrices, the scattering matrices $S^{J\pi}$ can be obtained [11,12]. They provide the elastic cross sections from the diagonal elements $S_{11}^{J\pi}$, by using standard formula of the scattering theory. The various transfer cross sections to channels c are obtained from

$$\left(\frac{d\sigma}{d\Omega}\right)_c = \frac{1}{10k^2} \sum_j B_{c,j}(E) P_j(\cos\theta), \tag{4}$$

where k is the wave number in the ^{8}Li + p entrance channel, $P_J(x)$ is a Legendre polynomial, and $B_{c,j}(E)$ are the anisotropy coefficients, directly deduced from the nondiagonal elements $S_{1c}^{J\pi}$ in the different partial waves (see Ref. [11], Sec. VIII). In Eq. (4), θ is the c.m. scattering angle.

The R-matrix code [12] was modified in order to include the channels, where the recoiling nuclei are in excited states. The center-of-mass energy above the reaction threshold was transformed into laboratory energy of the ejectiles, which are different when the recoil is excited, even if the resonance energy is the same. The present analysis involves five channels: proton ($c = 1$), α ($c = 2$), α' ($c = 3$), d ($c = 4$), and d' ($c = 5$), where α', and d' refer, respectively, to the recoiling nuclei ^{5}He and ^{7}Li in their first excited states. For the ^{8}Li$(p, \alpha)^{5}$He and ^{8}Li$(p, d)^{7}$Li cross sections, respectively, we have summed the R-matrix contributions of the ground and first excited states.

In the energy region close to the threshold, two resonances are important and described in the literature [28] at $E_{\text{c.m.}} = 0.41$ and 0.605 MeV, with tentative $J^\pi = (5/2)^-$ and $(7/2)^+$, and $\Gamma_{\text{total}} = 200$ and 47 keV values, respectively. We observed in our previous work [9] both resonances in the (p, α) channel, confirmed their energy and tentative spin/parity and suggested proton and α partial widths.

For the energy region between $E_{\text{c.m.}} = 1.0$–2.5 MeV, Ref. [28] indicates resonances at $E_{\text{c.m.}} = 1.13(5)$ MeV (observed in electron scattering), at 1.69(4) MeV [observed in the ^{7}Li$(d, p)^{8}$Li reaction], both without spin/parity or width attribution. The resonance at 1.76(5) MeV was observed in ^{9}Be$(p, p)^{9}$Be measurement [34] and $J^\pi = (3/2^+)$ and $\Gamma_{\text{total}} = 300 \pm 100$ keV was attributed. They did not observe the resonance at 1.69 MeV. Looking at their data it seems possible that they did not separate the close-lying resonances and their Γ_{total} refers to their superposition. The contribution of the decay of the hypernucleus $^{9}_{\Lambda}$Li, where a $T = 3/2$ state in ^{9}Be was observed at $E_{\text{c.m.}} = 1.7(1)$ MeV [35], motivated Tilley to attribute $J^\pi = (5/2^-)$ to the resonance at 1.76 MeV. Resonances were observed also at 2.31(5) MeV and 2.53(5) MeV, without spin/parity attributions and $\Gamma_{\text{total}} = 310 \pm 80$ keV and 600 ± 300 keV, respectively. These higher-lying resonances were not included in our calculations since they are out of our energy range, no experimental data exist for our reactions, and we do not know anything about their spin/parity and partial widths values. Our energy region is limited below 2.00 MeV. In all our experiments (see Fig. 6) we observed a large peak in the ^{8}Li$(p, \alpha)^{5}$He reaction around $E_{\text{c.m.}} = 1.6-1.75$ MeV, which probably corresponds to a superposition of the previously observed resonances at 1.69(4) MeV and 1.76(5) MeV.

In the R-matrix calculations of Ref. [9], besides the low-energy resonances ($E_r = 0.41$ and 0.65 MeV), two resonances were introduced to fit the peak at $E_{\text{c.m.}} = 1.7$ MeV, with energies and spins/parities, of $E_r = 1.69$ MeV, $J^\pi = 5/2^+$, and $E_r = 1.76$ MeV, $J^\pi = 7/2^+$. In this previous work only the excitation function of the ^{8}Li$(p, \alpha)^{5}$He reaction was measured and only Γ_p and Γ_α partial widths were considered. We began our calculations adopting the same resonance parameters, and allowing large variations of Γ_p, Γ_α, and Γ_d. Not only the elastic channel was impossible to reproduce in form and absolute value, but also the simultaneous fit of the ^{8}Li$(p, d)^{7}$Li and ^{8}Li$(p, \alpha)^{5}$He reactions was impossible. We also verified that the channel with excited ^{5}He* was unimportant, and thus we assumed $\Gamma_{\alpha'}$ ($c = 3$) to be negligible.

TABLE I. Resonance properties (energies in MeV, widths in keV) obtained from R-matrix fit. Energies are given with respect to the ^{8}Li + p threshold (16.888 MeV).

Present						Literature [28]		
E_r	J^π	Γ_p	Γ_α	Γ_d	$\Gamma_{d'}$	E_r	J^π	Γ
0.42 ± 0.007	$5/2^-$	40 ± 10	20 ± 3	150 ± 7[a]		0.41 ± 0.007	$(5/2)^-$	200
0.61 ± 0.007	$7/2^+$	1.0 ± 0.2	39 ± 4	7 ± 3		0.605 ± 0.007	$(7/2)^+$	47
1.10 ± 0.03	$3/2^+$	10 ± 7		30 ± 10	10 ± 5	1.13 ± 0.05		
1.65 ± 0.04	$7/2^-$	185 ± 10	185 ± 12	95 ± 7	30 ± 5	1.69 ± 0.04		
1.80 ± 0.04	$5/2^-$	20 ± 5	14 ± 2	25 ± 5	20 ± 5	1.76 ± 0.05	$(5/2^-)$	300 ± 100

[a]Fitted on the ^{7}Li(d, p)^{8}Li integrated cross section [33] near the resonance.

It is quite understandable that the inclusion of two or maybe three new decay channels strongly constrains the resonance parameters, and modifications are necessary to fit the new channels as well. We adjusted the R-matrix calculation only to our recent data, presented in Fig. 5.

A systematic search was performed, varying spins/parities and resonance parameters, in order to reproduce the elastic and the transfer cross sections. For the energy region around $E_{\text{c.m.}} = 1.6$–1.8 MeV, besides the resonances quoted in the literature [28] at $E_r = 0.41$ MeV, 0.605 MeV, 1.1 MeV, we began including only one resonance at energy $E_r = 1.65(4)$ MeV, with $J^\pi = 7/2^-$ and large Γ_α and Γ_d widths. We could get reasonable fits of the (p, p) and (p, α) channels and any other spin/parity attribution would not produce a minimum in (p, p) at the resonance energy. However, the double peak at E_d(reaction) = 7.1 and 7.8 MeV in the (p, d) data was not reproduced by this calculation. We included a second resonance at $E_r = 1.76$ MeV and varied all resonance parameters with the strong constraint of the form of the elastic cross section.

The best fit, which reproduced quite well all three excitation functions, was obtained assuming two resonances, one at $E_r = 1.65(4)$ MeV, with $J^\pi = 7/2^-$ and large Γ_p, Γ_α and Γ_d widths and the other at $E_r = 1.80(4)$ MeV, with $J^\pi = 5/2^-$, as suggested by Tilley *et al.*, with smaller partial widths. When using $J^\pi = 3/2^+$ as suggested by Ref. [34] for the second resonance, we had a much worse agreement for the absolute values. The parameters of the best fit calculation are presented in Table I, where we include also new information on the lower lying resonances. The energies of these two resonances agree within the uncertainties with the energies quoted in Ref. [28]. In our calculations we included a direct background, described by a $3/2^+$ resonance at $E_{\text{c.m.}} = 5.0$ MeV with $\Gamma_p = 10.4$ MeV and all other partial widths close to zero. The large partial widths Γ_p, Γ_α, and Γ_d of $E_r = 1.65(4)$ MeV are needed to reproduce the large width and absolute value of the peak in the ^{8}Li$(p, \alpha)^5$He cross section, and the depth and the absolute value of the minimum in the ^{8}Li(p, p)^{8}Li cross section.

Tilley *et al.* [28] quoted $T = 3/2$ for the higher-lying resonance, at $E_r = 1.80(4)$ MeV, and in this case the Γ_α and Γ_d widths should be zero, since ^{4}He + ^{5}He and ^{7}Li + d have $T = 1/2$. Effectively, in order to reproduce the much smaller width of the double peak in the ^{8}Li$(p, d)^7$Li cross section the resonance at $E_r = 1.80$ MeV has much smaller partial widths, however the double peak in (p, d) is mainly produced by the two channels, the ^{8}Li$(p, d)^7$Li and the ^{8}Li$(p, d)^7$Li* and thus both Γ_d and $\Gamma_{d'}$ need to be nonzero, indicating a possible isospin mixing in the $E_r = 1.80(4)$ MeV resonance. The result of the calculations is presented on Fig. 8. The reduced χ^2 of the multichannel calculation is 1.1.

The disagreement between the ^{8}Li$(p, \alpha)^5$He reaction data of Mendes *et al.* [9] and our recent data (see Fig. 6) can be better discussed in the light of the R-matrix calculations. One could argue that in the recent experiment we did not populate entirely the resonance at $E_r = 1.80(4)$ MeV and this is the origin of the difference in width and absolute value, observed in Fig. 6. However, in the measurements performed at 18.7 MeV, where this resonance is fully populated, the width of the peak agrees with our recent data of 16.0 MeV. Moreover, if the partial widths of the proton and α channels at $E_r = 1.80(4)$ MeV are increased to reproduce the previous data, the double peak in ^{8}Li$(p, d)^7$Li disappears and the fit of the ^{8}Li(p, p)^{8}Li gets much worse. The R-matrix calculation yields similar absolute values for the ^{8}Li$(p, \alpha)^5$He reaction at the three laboratory angles we have data points: 10.0°, 13.5°, and 18.0°. They correspond to $\theta_{\text{c.m.}} = 161.0°$, 154.3°, and 147.0°, respectively, for the (p, α) channel. The difference in absolute value between these experimental data is about 36%, even larger than the a $1/\sin(\theta_{\text{c.m.}})$ behavior, typical of thermalized compound nucleus. It is possible that a direct reaction contribution is responsible for the difference in the (p, α) cross sections.

The $5/2^-$ resonance near $E_{\text{c.m.}} = 0.41$ MeV determines the ^{8}Li(d, p)^{7}Li cross section at low energies [33], and is used to normalize the ^{7}Be$(p, \gamma)^8$B cross section [36]. We started from Γ_p and Γ_d values, which reproduce the cross section near this resonance, and adjusted Γ_α to account for the structure in the ^{8}Li$(p, \alpha)^5$He cross section at low energies [9].

From the R-matrix partial widths of the two close-lying resonances, we calculated the reduced widths γ^2 and the dimensionless reduced widths θ^2 for the α and d channels. The θ_α^2 values of the resonances at 1.65 and 1.80 MeV are, respectively, 1.4(1)% and 0.11(2)%. However, the resonance at 1.65 MeV, with $J^\pi = 7/2^-$ and $\ell = 2$ has $\theta_d^2 = 7.4(6)$%, which indicates a strong ^{7}Li + d clustering in this state, similar to the $E_r = 0.42$ MeV resonance, which has $\theta_d^2 = 10.5(5)$%.

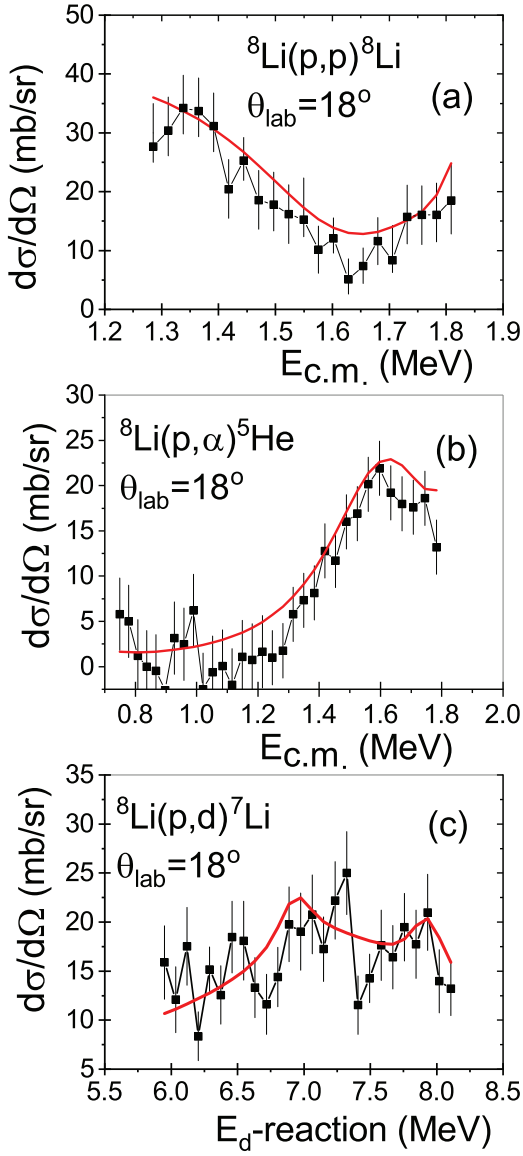

FIG. 8. The experimental cross sections of the reactions ^{8}Li$(p, p)^8$Li [in (a)], ^{8}Li$(p, \alpha)^5$He [in (b)], ^{8}Li$(p, d)^7$Li [in (c)] measured at $\theta_{\rm lab} = 18^\circ$ with $E_{\rm lab} = 16.0$ MeV. The red solid line is the result of the best fit R-matrix calculation using the resonance parameters presented on Table I and was obtained including excitation of the recoiling ^{7}Li in the reaction ^{8}Li$(p, d)^7$Li. More details and explanations in the text.

V. CONCLUSIONS

We have performed a simultaneous measurement of the ^{8}Li$(p, p)^8$Li, ^{8}Li$(p, d)^7$Li, and ^{8}Li$(p, \alpha)^5$He cross sections at low energies. The data measured at the laboratory angle $\theta_{\rm lab} = 18^\circ$, where the possible contamination had very low yield, allowed us to measure accurately the absolute values of the cross sections of elastic scattering and transfer reactions. The availability of the three cross sections, and in particular of the elastic cross section, puts constraints on the R-matrix fits. With a common set of R-matrix parameters assuming two resonances, one at $E_r = 1.65(4)$ MeV, with $J^\pi = 7/2^-$ and large Γ_p, Γ_α, and Γ_d widths and the other at $E_r = 1.80(4)$ MeV, with $J^\pi = 5/2^-$, with smaller partial widths, the three cross sections can be fitted well, with a reduced χ^2 of 1.1. These resonances should correspond to the resonances previously observed and presented in Ref. [28] at $E_r = 1.69(4)$ MeV and 1.76(5) MeV since the energies agree within the uncertainties. In the ^{8}Li$(p, d)^7$Li data we see two peaks, which strongly constrain not only the energies but also the partial widths of the two close-lying resonances needed to give a good fit to the data. The ^{8}Li$(p, d)^7$Li and ^{8}Li$(p, d)^7$Li* reactions leading to ^{7}Li$_{\rm gs}$ and its first excited state at 0.4776 MeV are necessary to describe the double peak in the ^{8}Li$(p, d)^7$Li data.

The dimensionless reduced widths θ^2 for the α channel of the resonances at 1.65 and 1.80 MeV are, respectively, 1.4(1)% and 0.11(2)%. However, for the d channel the resonance at 1.65 MeV, with $J^\pi = 7/2^-$ and $\ell = 2$ has $\theta_d^2 = 7.4(6)\%$, which indicates a strong $^7{\rm Li} + d$ clustering in this state, similar to the $E_r = 0.42$ MeV resonance, which has $\theta_d^2 = 10.5(5)\%$. The ^{7}Li ground state shows a strong clustering in $\alpha + t$ and the weakly bound deuteron can be described as constituted by two cores, a proton and a neutron. Thus, the ^{8}Li$(p, d)^7$Li data suggest a four-body $\alpha + t + p + n$ resonance near $E_x = 18.55 \pm 0.04$ MeV in ^{9}Be. Its theoretical interpretation is a challenge for cluster models, and it certainly deserves further experimental and theoretical studies. In particular, a similar resonance with $\ell = 0$ should exist at lower energies.

ACKNOWLEDGMENTS

This work was supported by Fundação de Amparo à Pesquisa do Estado de São Paulo (FAPESP) proc. No. 2011/15904-7, 2013/22100-7 and 2016/21434-7, by Conselho Nacional de Desenvolvimento Cientifico e Tecnologico (CNPq) and Comissão de Aperfeiçoamento do Ensino Superior (CAPES). M.A.G.A. would like to thank the VI Plan Propio de Investigacin - Universidad de Sevilla (2017–2018). We thank P. Descouvemont for the modification of his R-matrix code and help during part of the calculations.

APPENDIX

Our goal in this Appendix is to discuss possible contamination in our data, but also to show that the TTIK method can be used with exotic beams produced by the in-flight method, however, it demands a very careful analysis of all possible contaminant reactions. Light particles can appear in the energy spectra also from spurious reactions on the $[CH_2]_n$ target. For the measurements performed at $\theta_{\rm lab} = 18^\circ \pm 2^\circ$ and $E_{\rm inc}(^8{\rm Li}) = 16.0$ MeV we consider the beam of interest ^{8}Li and the main contaminant beams, visible on Fig. 3 (middle), ^{4}He and ^{3}H. The amounts of ^{4}He and ^{3}H with respect to ^{8}Li are, respectively, 0.69% and 0.9%, as measured on the gold target. The energies available are $E_{\rm lab}(^8{\rm Li}) =$ 16.0–0 MeV, as the ^{8}Li stops in the target. The ^{4}He beam has incident energy between 17–18 MeV, and considering its energy loss in the $[CH_2]_n$/carbon targets, respectively, it can produce reactions with energy between $E_{\rm lab}(\alpha) =$ 18–14

TABLE II. Available information on the energy range in the detectors of all possible contaminant reactions that can occur between ^{8}Li, α, triton, and deuteron beams on the $[CH_2]_n$ target. The energy losses of the beams and of the ejectiles in the target are taken into account. Energies are expressed in MeV.

Contaminant reactions affecting the proton spectrum								
Reactions	Q_{gs}	θ_{lab}	$E_{lab}(^{8}Li)$	$E_{lab}(\alpha)$	$E_{lab}(t)$	$E_{lab}(d)$	E_p(det)	Observed?
$^{1}H(\alpha, p)^{4}He$	0	18°	–	18–14	–	–	10.5–7.9	Yes
$^{1}H(t, p)^{3}H$	0	18°	–	–	6–5	–	3.3	No
$^{1}H(t, p)^{3}H$	0	18°	–	–	12–11	–	7.8	Yes
$^{12}C(^{8}Li, p)^{19}O$	+10.32	18°	16.0–0	–	–	–	23–10	No
$^{12}C(\alpha, p)^{15}N$	−4.9	18°	–	18–14	–	–	10.7–7.3	Yes
$^{12}C(t, p)^{14}C$	+4.65	18°	–	–	6–5	–	10–8.6	Yes
$^{12}C(t, p)^{14}C$	+4.65	18°	–	–	12–11	–	15.5–15.3	No
Contaminant reactions affecting the deuteron spectrum								
Reactions	Q_{gs}	θ_{lab}	$E_{lab}(^{8}Li)$	$E_{lab}(\alpha)$	$E_{lab}(t)$	$E_{lab}(d)$	E_d(det)	Observed?
$^{1}H(\alpha, d)^{3}He$	−18.35	10°	–	16.6–13	–	–	–	No
$^{1}H(\alpha, d)^{3}He$	−18.35	18°	–	18–14	–	–	–	No
$^{1}H(t, d)^{2}H$	−4.03	10°	–	–	5.1–3.5	–	–	No
$^{1}H(t, d)^{2}H$	−4.03	10°	–	–	14.2–13.5	–	–	No
$^{1}H(t, d)^{2}H$	−4.03	18°	–	–	6–5	–	–	No
$^{1}H(t, d)^{2}H$	−4.03	18°	–	–	12–11	–	–	No
$^{1}H(d, d)^{1}H$	0	10°	–	–	–	8.3–7.5	7.8–7.0	No
$^{12}C(^{8}Li, d)^{18}O$	+8.59	10°	18.7–0	–	–	–	25.7–7.7	No
$^{12}C(^{8}Li, d)^{18}O$	+8.59	18°	16.0–0	–	–	–	23–7.7	No
$^{12}C(\alpha, d)^{15}N$	−13.57	10°	–	16.6–13	–	–	–	No
$^{12}C(\alpha, d)^{15}N$	−13.57	18°	–	18–14	–	–	–	No
$^{12}C(t, d)^{13}C$	−1.31	10°	–	–	5.1–3.5	–	3.6–2	No
$^{12}C(t, d)^{13}C$	−1.31	10°	–	–	14.2–13.5	–	12.6–12	No
$^{12}C(t, d)^{13}C$	−1.31	18°	–	–	6–5	–	3.5–2	No
$^{12}C(t, d)^{13}C$	−1.31	18°	–	–	12–11	–	10–9	No
$^{12}C(d, d)^{12}C$	0	10°	–	–	–	8.3–7.5	8.2–7.6	No
Contaminant reactions affecting the alpha spectrum								
Reactions	Q_{gs}	θ_{lab}	$E_{lab}(^{8}Li)$	$E_{lab}(\alpha)$	$E_{lab}(t)$	$E_{lab}(d)$	E_α(det)	Observed?
$^{1}H(\alpha, \alpha)^{1}H$	0	10°	–	16.6–13	–	–	14.4–11.3	No
$^{1}H(\alpha, \alpha)^{1}H$	0	18°	–	18–14	–	–	–	No
$^{1}H(t, \alpha)$	19.81	10°	–	–	5.1–3.5	–	–	No
$^{1}H(t, \alpha)$	19.81	10°	–	–	14.2–13.5	–	–	No
$^{1}H(t, \alpha)$	19.81	18°	–	–	5–6	–	–	No
$^{1}H(t, \alpha)$	19.81	18°	–	–	11–12	–	–	No
$^{12}C(^{8}Li, \alpha)^{16}N$	+12.37	10°	18.7–0	–	–	–	31.2–10.4	Yes
$^{12}C(^{8}Li, \alpha)^{16}N$	+12.37	18°	16.0–0	–	–	–	28.1–10.4	No
$^{12}C(\alpha, \alpha)^{12}C$	0	10°	–	16.6–13	–	–	16–12.5	Yes
$^{12}C(\alpha, \alpha)^{12}C$	0	18°	–	18–14	–	–	17.4–13.5	Yes
$^{12}C(t, \alpha)^{11}B$	+3.86	10°	–	–	5.1–3.4	–	8.5–9	No
$^{12}C(t, \alpha)^{11}B$	+3.86	10°	–	–	14.2–13.5	–	15–14.5	No
$^{12}C(t, \alpha)^{11}B$	+3.86	18°	–	–	6–5		9–8.5	No
$^{12}C(t, \alpha)^{11}B$	+3.86	18°	–	–	12–11		15–14.5	No
$^{12}C(d, \alpha)^{11}B$	−1.34	10°	–	–	–	8.3–7.5	6.8–5.9	No

MeV/18–11.5 MeV on the $[CH_2]_n$/carbon targets. We observe on Fig. 1, middle, two contaminant beams of tritons with energies $E_{lab}(t) = 6$–5 MeV and 12–11 MeV.

For the measurements performed at $\theta_{lab} = 10° \pm 2.5°$ and $E_{inc}(^{8}Li) = 18.7$ MeV we have used a $[CH_2]_n$ degrader in chamber (2) and the proton spectrum was completely polluted by recoiling protons from the degrader. Also due to the very forward angle we had strong contaminant beams of deuterons, tritons, and α particles with energies of, respectively, $E_{lab}(d) = 8.3$–7.5 MeV, two contaminant beams of tritons with energies $E_{lab}(t) = 5.1$–3.5 MeV and 14.2–13.5 MeV and $E_{lab}(\alpha) = 16.6$–13 MeV.

We calculated the range of energies of protons, deuterons, α ejectils produced in all possible reactions detected at $\theta_{lab} = 10° \pm 2.5°$ and $18° \pm 2°$ and in Table II we summarize all information about possible contamination of our proton, deuteron, and α spectra.

Referring to data measured at 18°, the reactions produced by the α and triton beams on the protons and carbons of the $[CH_2]_n$ target explain the yield we observe on our

proton spectra with energies $E_p(\text{det}) \geqslant 5.2$ MeV, which is the kinematic limit of the ^{8}Li$(p, p)^8$Li reaction of interest. In Ref. [37] we found experimental data on ^{4}He$(p, p)^4$He elastic scattering angular distributions, for E_p between 2–11 MeV. The cross section for E_α between 14–18 MeV varies from 650 mb/sr to 400 mb/sr. Even with the very small amount of α beam this reaction fully explains the yield we observe for E_p between 7.9 and 10.5 MeV. Luckily, at this energy and angle, the $p + \alpha$ elastic scattering does not superimpose on our reaction of interest. The elastic scattering of the triton beam with energies 5–6 MeV and 11–12 MeV on protons should yield well-defined peaks in the proton spectrum at 3.3 and 7.8 MeV. Effectively, there is a small peak, out of our range of interest, at 7.8 MeV.

The reaction ^{12}C$(\alpha, p)^{15}$N has $Q_{g.s.}$ value of -4.9 MeV and optimum Q-value of -6.6 MeV, thus probably the reaction goes through the ground state. On the thick ^{12}C target of 15 mg/cm^2 it can produce protons with energies between 5 and 10.4 MeV, which is the strip we see in Fig. 1 (bottom). However, on the thinner $[CH_2]_n$ target the protons have higher energies, between 7.3 and 10.7 MeV. As none of the contaminant reactions on carbon contribute in the energy range of interest, we did not subtract the proton spectrum measured with carbon target from our data measured with the $[CH_2]_n$ target.

The conclusion about the reactions that can produce protons in our range of interest are: there is no contamination in our range of measurements between $E_p(\text{detector}) = 3.5-5.15$ MeV, however the protons we observe with energies between 5.15 and 10.5 MeV can come from ^{1}H$(\alpha, p)^4$He, ^{1}H$(t, p)^3$H, and ^{12}C$(\alpha, p)^{15}$N reactions. The fact that the proton strip goes up to 10.5 MeV indicates that the reactions go mainly through the ground states. The conclusions about the contamination of the deuteron spectrum are: as the maximum detected energy is about 7.5 MeV, none of the contaminant reactions are important. This conclusion is also supported by the very low yield of deuterons (and alphas) on the carbon target, which had similar number of incident particles and which is thicker in carbon than the $[CH_2]_n$ target. The same argument supports that the α spectrum is also free from contamination. α particles produced with energy below 18 MeV are out of the region measured with purified ^{8}Li beam, presenting no harm to our data.

Referring to data measured at 10°, the deuteron spectrum has a strong peak between $E_d(\text{detector}) = 7.0$–$7.8$ MeV, due to ^{1}H$(d, d)^1$H reaction. The contribution from the ^{12}C$(^8\text{Li}, \alpha)^{16}$N reaction on the α-particle spectrum was subtracted by using data measured with the carbon target [9].

[1] I. Tanihata, H. Savajols, and R. Kanungo, Prog. Part. Nucl. Phys. **68**, 215 (2013).
[2] S. Gales, Prog. Part. Nucl. Phys. **59**, 22 (2007).
[3] T. Motobayashi, Prog. Part. Nucl. Phys. **59**, 32 (2007).
[4] A. Lépine-Szily, R. Lichtenthäler, and V. Guimarães, Eur. Phys. J. A **50**, 128 (2014).
[5] C. Bertulani and A. Gade, Phys. Rep. **485**, 195 (2010).
[6] M.-G. Pellegriti, N. L. Achouri, C. Angulo, J. C. Angelique, E. Berthoumieux, E. Casarejos, M. Couder, T. Davinson, C. Ghag, A. S. Murphy, N. A. Orr, I. Ray, I. G. Stefan, and P. Descouvemont, Phys. Lett. B **659**, 864 (2008).
[7] A. M. Moro and R. Crespo, Phys. Rev. C **85**, 054613 (2012).
[8] A. Deltuva, Phys. Rev. C **88**, 011601 (2013).
[9] D. R. Mendes, Jr., A. Lépine-Szily, P. Descouvemont, R. Lichtenthäler, V. Guimarães, P. N. de Faria, A. Barioni, K. C. C. Pires, V. Morcelle, R. Pampa Condori, M. C. Morais, E. Leistenschneider, C. E. F. Lima, J. C. Zamora, J. A. Alcantara, V. Zagatto, M. Assunção, and J. M. B. Shorto, Phys. Rev. C **86**, 064321 (2012). (See Erratum [10].)
[10] D. R. Mendes, Jr., A. Lépine-Szily, P. Descouvemont, R. Lichtenthäler, V. Guimarães, P. N. de Faria, A. Barioni, K. C. C. Pires, V. Morcelle, R. Pampa Condori, M. C. Morais, E. Leistenschneider, C. E. F. Lima, J. C. Zamora, J. A. Alcantara, V. Zagatto, M. Assunção, and J. M. B. Shorto, Phys. Rev. C **98**, 069901(E) (2018). (Erratum to [9].)
[11] A. M. Lane and R. G. Thomas, Rev. Mod. Phys. **30**, 257 (1958).
[12] P. Descouvemont and D. Baye, Rep. Prog. Phys. **73**, 036301 (2010).
[13] E. A. Benjamim, A. Lépine-Szily, D. R. Mendes, Jr., R. Lichtenthäler, V. Guimarães, P. R. S. Gomes, L. C. Chamon, M. S. Hussein, A. M. Moro, A. Arazi, I. Padron, J. A. Nunez, M. Assuncao, A. Barioni, O. Camargo, Jr., R. Z. Denke, P. N. de Faria, and K. C. C. Pires, Phys. Lett. B **647**, 30 (2007).
[14] R. Lichtenthäler, M. A. G. Alvarez, A. Lépine-Szily, S. Appannababu, K. C. C. Pires, U. U. da Silva, V. Scarduelli, R. P. Condori, and N. Deshmukh, Few-Body Systems **57**, 157 (2016).
[15] E. Leistenschneider, A. Lépine-Szily, and R. Lichtenthäler, AIP Conf. Proc. **1529**, 206 (2013).
[16] A. Lépine-Szily, R. Lichtenthäler, and RIBRAS Collaboration, Nucl. Phys. A **787**, 94 (2007).
[17] K. C. C. Pires, R. Lichtenthäler, A. Lépine-Szily, V. Guimarães, P. N. de Faria, A. Barioni, D. R. Mendes Junior, V. Morcelle, R. Pampa Condori, M. C. Morais, J. C. Zamora, E. Crema, A. M. Moro, M. Rodríguez-Gallardo, M. Assuncao, J. M. B. Shorto, and S. Mukherjee, Phys. Rev. C **83**, 064603 (2011).
[18] V. Morcelle, K. C. C. Pires, M. Rodríguez-Gallardo, R. Lichtenthäler, A. Lépine-Szily, V. Guimarães, P. N. de Faria, D. R. Mendes, Jr., A. M. Moro, L. R. Gasques, E. Leistenschneider, R. Pampa Condori, V. Scarduelli, M. C. Morais, A. Barioni, J. C. Zamora, and J. M. B. Shorto, Phys. Lett. B **732**, 228 (2014).
[19] J. C. Zamora, V. Guimarães, A. Barioni, A. Lépine-Szily, R. Lichtenthäler, P. N. de Faria, D. R. Mendes, L. R. Gasques, J. M. B. Shorto, V. Scarduelli, K. C. C. Pires, V. Morcelle, E. Leistenschneider, R. P. Condori, V. A. Zagatto, M. C. Morais, and E. Crema, Phys. Rev. C **84**, 034611 (2011).
[20] P. N. de Faria, R. Lichtenthäler, K. C. C. Pires, A. M. Moro, A. Lépine-Szily, V. Guimarães, D. R. Mendes, Jr., A. Arazi, A. Barioni, V. Morcelle, and M. C. Morais, Phys. Rev. C **82**, 034602 (2010).
[21] P. N. de Faria, R. Lichtenthäler, K. C. C. Pires, A. M. Moro, A. Lépine-Szily, V. Guimarães, D. R. Mendes, Jr., A. Arazi, M.

Rodríguez-Gallardo, A. Barioni, V. Morcelle, M. C. Morais, O. Camargo, Jr., J. Alcantara Nuñez, and M. Assunção, Phys. Rev. C **81**, 044605 (2010).

[22] S. Mukherjee, N. N. Deshmukh, V. Guimarães, J. Lubian, P. R. S. Gomes, A. Barioni, S. Appannababu, C. C. Lopes, E. N. Cardozo, K. C. C. Pires, R. Lichtenthäler, A. Lépine-Szily, D. S. Monteiro, J. M. B. Shorto, P. N. de Faria, E. Crema, V. Morcelle, M. C. Morais, and R. Pampa Condori, Eur. Phys. J. A **45**, 23 (2010).

[23] A. Barioni, V. Guimarães, A. Lépine-Szily, R. Lichtenthäler, D. R. Mendes, E. Crema, K. C. C. Pires, M. C. Morais, V. Morcelle, P. N. de Faria, R. P. Condori, A. M. Moro, D. S. Monteiro, J. M. B. Shorto, J. Lubian, and M. Assunção, Phys. Rev. C **80**, 034617 (2009).

[24] V. Morcelle, R. Lichtenthäler, A. Lépine-Szily, V. Guimarães, K. C. C. Pires, J. Lubian, D. R. Mendes Junior, P. N. de Faria, J. J. Kolata, F. D. Becchetti, H. Jiang, E. F. Aguilera, D. Lizcano, E. Martinez-Quiroz, and H. Garcia, Phys. Rev. C **95**, 014615 (2017).

[25] V. Morcelle, R. Lichtenthäler, R. Linares, M. C. Morais, V. Guimarães, A. Lépine-Szily, P. R. S. Gomes, J. Lubian, D. R. Mendes Junior, P. N. De Faria, A. Barioni, L. R. Gasques, J. M. B. Shorto, K. C. C. Pires, J. C. Zamora, R. P. Condori, V. Scarduelli, J. J. Kolata, H. Amro, F. D. Becchetti, H. Jiang, E. F. Aguilera, D. Lizcano, E. Martinez-Quiroz, and H. Garcia, Phys. Rev. C **89**, 044611 (2014).

[26] K. C. C. Pires, R. Lichtenthäler, A. Lépine-Szily, and V. Morcelle, Phys. Rev. C **90**, 027605 (2014).

[27] E. Leistenschneider, *Proton-Induced Reactions on ^{8}Li at Low Energies and Spectroscopy of ^{9}Be at High Excitation Energies*, Master's Dissertation in Physics, Instituto de Física (University of São Paulo, São Paulo, 2014).

[28] D. R. Tilley, J. H. Kelley, J. L. Godwin, D. J. Millener, J. E. Purcell, C. G. Sheu, and H. R. Weller, Nucl. Phys. A **745**, 155 (2004).

[29] Y.-J. Li, Z.-H. Li, B. Guo, Y.-B. Wang, X.-X. Bai, S. Zeng, B.-X. Wang, X. Quin, C. Jiang, L. Wei-Ping, and W.-J. Zhao, Chin. Phys. Lett. **25**, 455 (2008).

[30] J. P. Mitchell, G. V. Rogachev, E. D. Johnson, L. T. Baby, K. W. Kemper, A. M. Moro, P. Peplowski, A. S. Volya, and I. Wiedenhöver, Phys. Rev. C **87**, 054617 (2013).

[31] P. Descouvemont, Eur. Phys. J. A **12**, 413 (2001).

[32] C. R. Brune, Phys. Rev. C **66**, 044611 (2002).

[33] S. Bashkin, Phys. Rev. **95**, 1012 (1954).

[34] S. Dixit, W. Bertozzi, T. N. Buti, J. M. Finn, F. W. Hersman, C. E. Hyde-Wright, M. V. Hynes, M. A. Kovash, B. E. Norum, J. J. Kelly, A. D. Bacher, G. T. Emery, C. C. Foster, W. P. Jones, D. W. Miller, B. L. Berman, and D. J. Millener, Phys. Rev. C **43**, 1758 (1991).

[35] J. Pniewski, K. Garbowska-Pniewska, D. Kiełczewska, D. Davis, G. Bohm, U. Krecker, A. Montwill, P. Moriarty, G. Coremans-Bertrand, J. Sacton, and M. Jurič, Nucl. Phys. A **443**, 685 (1985).

[36] B. W. Filippone, A. J. Elwyn, C. N. Davids, and D. D. Koetke, Phys. Rev. C **28**, 2222 (1983).

[37] A. C. L. Barnard, C. M. Jones, and J. L. Weil, Nucl. Phys. **50**, 604 (1964).